VII International Conference on Computational Methods for Coupled Problems in Science and Engineering
COUPLED PROBLEMS 2017
M. Papadrakakis, E. Oñate and B. Schrefler (Eds)

REDUCED-ORDER HYBRID MULTISCALE METHOD COMBINING THE MOLECULAR DYNAMICS AND THE DISCONTINUOUS-GALERKIN METHOD

N. Emamy[†], M. Lukáčová-Medvid'ová[†], S. Stalter[‡], P. Virnau[‡], L. Yelash[*†]

[†] Institute of Mathematics, Johannes Gutenberg-Universität,
Staudingerweg 9, 55128 Mainz, Germany
emamy@mathematik.uni-mainz.de, lukacova@uni-mainz.de, yelash@uni-mainz.de

[‡] Institute of Physics, Johannes Gutenberg-Universität,
Staudingerweg 9, 55128 Mainz, Germany
ststalte@uni-mainz.de, virnau@uni-mainz.de

Key words: Numerical Methods, Multi-Scale, discontinuous Galerkin, HMM, CFD, Molecular Dynamics

Abstract. We present a new reduced-order hybrid multiscale method to simulate complex fluids. The method combines the continuum and molecular descriptions. We follow the framework of the heterogeneous multi-scale method (HMM) that makes use of the scale separation into macro- and micro-levels. On the macro-level, the governing equations of the incompressible flow are the continuity and momentum equations. The equations are solved using a high-order accurate discontinuous Galerkin Finite Element Method (dG) and implemented in the BoSSS code. The missing information on the macro-level is represented by the unknown stress tensor evaluated by means of the molecular dynamics (MD) simulations on the micro-level. We shear the microscopic system by applying Lees-Edwards boundary conditions and either an isokinetic or Lowe-Andersen thermostat. The data obtained from the MD simulations underlie large stochastic errors that can be controlled by means of the least-square approximation. In order to reduce a large number of computationally expensive MD runs, we apply the reduced order approach. Numerical experiments confirm the robustness of our newly developed hybrid MD-dG method.

1 Introduction

The most accurate description of complex fluids can be obtained by the molecular dynamics. However, such microscale description is computationally inefficient if large scale regions in space and time need to be simulated. To overcome this restriction and to obtain practically tractable simulation techniques suitable combinations of macroscopic and microscopic models have been proposed in the literature. A hybrid molecular-continuum

approach aims in combining the best attributes of both parts: it combines molecular accuracy with the computational efficiency of continuum models. In the case when processes occurring on a small scale are only loosely coupled with the behavior on a much larger scale and the so-called *scale separation* occurs, the hybrid schemes known in the literature as the *Heterogeneous Multiscale Methods* (HMM) have been successfully used, see, e.g., [1, 2, 3, 4, 5] and the references therein.

In this paper we present a novel hybrid multiscale method that is based on the combination of the discontinuous Galerkin (dG) method and molecular dynamics (MD) in order to simulate complex fluids, such as colloids in a Newtonian solvent. The main aim of the present study is two-fold: we use (i) modern numerical method for macroscopic flow equations which allows more flexible discretization including per-cell momentum conservation as well as (ii) the reduced order techniques in order to control the number of needed but computationally expensive MD simulations. As far as we know this is *the first study* implementing techniques (i) and (ii) within the HMM framework. Consequently, our main goal is to increase the accuracy as well as efficiency of this very attractive multiscale simulation framework.

2 Particle model

To simulate colloids, we use non-equilibrium Molecular Dynamics (MD) [6]. The colloids are treated as hard spheres with the interaction modelled using a Weeks-Chandler-Andersen (WCA) potential, which corresponds to the repulsive part of a cut and shifted Lennard-Jones potential

$$V_{WCA} = 4\varepsilon \left[\left(\frac{\sigma}{r}\right)^{12} - \left(\frac{\sigma}{r}\right)^{6} + \frac{1}{4} \right] \ , \quad r < r_c = \sqrt[6]{2}\sigma \ , \text{ else } V_{WCA} = 0 \ , \tag{1}$$

where r is the distance between two particles, r_c the cut-off distance, ϵ the well depth of the Lennard-Jones potential (in our case, $\epsilon = kT$), σ the typical radius of a colloid used as the length scale of the MD simulations.

The MD simulations are performed using the velocity Verlet time integration, which yields a Hamiltonian preserving second order approximation, with the standard Lees-Edwards periodic boundary conditions [7] for an one-dimensional shear flow, see Figure 1a. The temperature is preserved by using a thermostat. We employed the momentum conserving, Galilean invariant, Lowe-Andersen thermostat (LAT) [8]. For high shear rates, this thermostat needs a long relaxation time, therefore we also employed the isokinetic thermostat (ISO) with the SLLOD method [9], see Figure 1b.

The important quantity we obtain from the particle based model is the stress tensor calculated via the Irving-Kirkwood formula [10] using peculiar velocities of particles $\mathbf{v}_i = \tilde{\mathbf{v}}_i - \mathbf{v}_{i,s}$, where $\tilde{\mathbf{v}}_i$ is the total and $\mathbf{v}_{i,s}$ the streaming velocity of particle i, respectively,

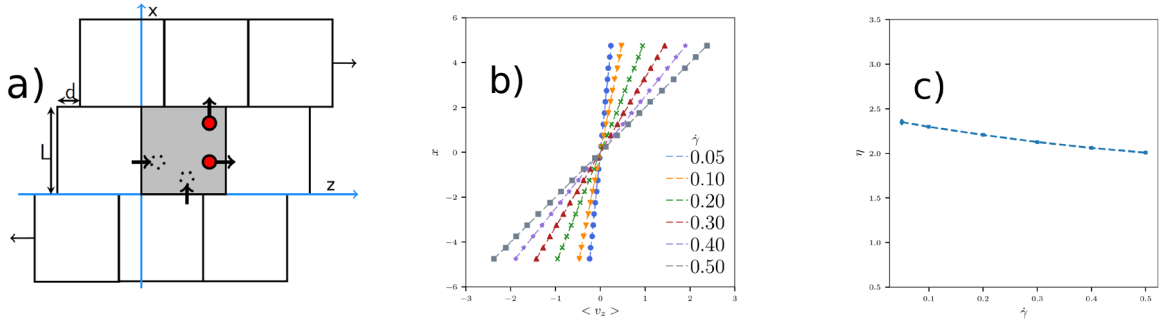

Figure 1: a) Lees-Edwards boundary conditions; b) Shear profiles for different shear rates with the isokinetic thermostat and the SLLOD algorithm for a density of $\rho = 0.8442$ after 1 000 MD-times; c) The viscosity of the system with density $\rho = 0.8442$.

$$\sigma_{\alpha\beta}(t) = -\frac{1}{V}\left(\sum_{i}^{N}(m_i v_{i,\alpha} v_{i,\beta}) + \sum_{i}^{N}\sum_{j>i}^{N} r_{ij,\alpha} F_{ij,\beta}\right). \tag{2}$$

The mean stress is $\pi = Tr(\sigma)/n$ with $n = \{2, 3\}$ the number of space dimensions. From the stresses we calculate the fluid pressure as $p = -\pi_{\dot{\gamma}=0}$ and the dynamic viscosity $\eta = |\sigma_{xz}/\dot{\gamma}|$. As indicated by Figure 1c, the simulated fluid is weakly non-Newtonian.

3 Continuum model

3.1 Governing equations

At the macroscopic level, the motion of the incompressible fluid flow is governed by the continuity and momentum equations,

$$\nabla \cdot \mathbf{u} = 0, \qquad \text{in } \Omega \times [0, t_F] \tag{3a}$$

$$\rho\left(\frac{\partial \mathbf{u}}{\partial t} + \mathbf{u} \cdot \nabla \mathbf{u}\right) = \frac{1}{Re}\nabla \cdot \boldsymbol{\sigma} + \mathbf{g}, \qquad \text{in } \Omega \times [0, t_F] \tag{3b}$$

$$\mathbf{u} = \mathbf{u}_D, \qquad \text{on} \quad \partial\Omega_D \tag{3c}$$

$$\mathbf{u}(t = 0) = \mathbf{u}^{(0)} \qquad \text{in } \Omega, \tag{3d}$$

where $\mathbf{u}$ is the velocity vector, $\boldsymbol{\sigma}$ the Cauchy stress tensor, $\mathbf{g}$ an external body force, ρ the density and Re the Reynolds number. The computational domain Ω is surrounded by the boundary $\partial\Omega = \partial\Omega_D \cup \partial\Omega_P$, where the Dirichlet and periodic boundaries are considered, respectively. In case of the Navier-Stokes equations for Newtonian fluids, $\boldsymbol{\sigma} = -p\mathbf{I} + \boldsymbol{\tau}$, where $\boldsymbol{\tau} = \mu(\nabla \mathbf{u} + \nabla \mathbf{u}^T)$, the above momentum equations reduce to

$$\rho\left(\frac{\partial \mathbf{u}}{\partial t} + \mathbf{u} \cdot \nabla \mathbf{u}\right) = -\nabla p + \frac{1}{Re}(\mu \Delta \mathbf{u}) + \mathbf{g} \quad \text{in } \Omega. \tag{4}$$

3.2 Time integration

For the time integration of the continuity equation (3a) and momentum equations (3b) we apply the following multi-step projection method. Using the first-order Euler method we have

$$\text{I} \quad \tilde{\mathbf{u}} = \Delta t\Big(- \mathbf{u}^{(n)} \cdot \nabla \mathbf{u}^{(n)} + \frac{1}{Re}\nabla \cdot (\boldsymbol{\sigma}^{(n)}/\rho) + \mathbf{g}^{(n)}/\rho\Big), \quad \text{in } \Omega \tag{5a}$$

$$\text{II} \quad \Delta \bar{p}^{(n+1)} = \nabla \cdot \Big(\tilde{\mathbf{u}}/\Delta t\Big), \quad \text{in } \Omega \tag{5b}$$

$$\frac{\partial \bar{p}}{\partial \mathbf{n}}^{(n+1)} = \mathbf{n} \cdot \Big(\tilde{\mathbf{u}}/\Delta t\Big), \quad \text{on } \partial\Omega \tag{5c}$$

$$\tilde{\tilde{\mathbf{u}}} = \tilde{\mathbf{u}} - \Delta t \nabla \bar{p}^{(n+1)}, \quad \text{in } \Omega \tag{5d}$$

$$\text{III} \quad \mathbf{u}^{(n+1)} = \mathbf{u}^{(n)} + \tilde{\tilde{\mathbf{u}}}, \quad \text{in } \Omega. \tag{5e}$$

Here we define the average pressure $\bar{p}^{(n+1)} = 1/\Delta t \int_{t^n}^{t^{n+1}} p'/\rho \, dt$ with the normal derivative $\partial \bar{p}^{(n+1)}/\partial \mathbf{n} = \mathbf{n} \cdot \nabla \bar{p}^{(n+1)}$. To obtain a unique solution for (5b)-(5c), we require $\int_\Omega \bar{p}^{(n+1)} = 0$. Note that p' is a correction to the pressure to ensure the divergence-free constraint. As one notices, the pressure is already present in the stress tensor in equation (3b). For the second-order time integration of the velocity, we use the Adams-Bashforth method in the first step I,

$$\tilde{\mathbf{u}}_{AB} = \Delta t \sum_{j=0}^{J-1} \beta_j \Big(- \mathbf{u}^{(n-j)} \cdot \nabla \mathbf{u}^{(n-j)} + \frac{1}{Re}\nabla \cdot (\boldsymbol{\sigma}^{(n-j)}/\rho) + \mathbf{g}^{(n-j)}/\rho\Big),$$

with the coefficients $\beta_0 = 3/2$ and $\beta_1 = -1/2$. However, the effective pressure, $\bar{p}^{(n+1)}$, is first-order accurate in time. If required, one can reconstruct the pressure for higher-order accuracy, see [11, 12]. In the above Chorin projection scheme, we use by construction $\nabla \cdot \mathbf{u}^{(n-j)} = 0$, for all $j \geq 0$, which is suggested in [13]. Therefore, we can integrate the unsteady terms in the third step III. In this way, by replacing the intermediate velocity from the first step, the right-hand side of the Poisson equation in the second step II is independent of the time step. This prevents the numerical instability observed in [14, 15, 16] using the dG method.

3.3 Spatial discretization

Following the notations and definitions in [17], we use a matching simplicial geometry-conforming mesh $\mathcal{T}_h$ with mesh size h on the domain Ω. For a mesh element T, $\mathbf{n}_T$ is the unit outward normal to T on the boundary ∂T. Mesh faces $\mathcal{F}_h$ can be either the inner interfaces between adjacent elements $\mathcal{F}_h^i$ or boundary faces $\mathcal{F}_h^b$. The face normal $\mathbf{n}_\mathcal{F}$ points from an arbitrarily chosen (but fixed) element T_1 towards T_2. Therefore, $\mathbf{n}_\mathcal{F} = \mathbf{n}_{T_1} = -\mathbf{n}_{T_2}$ on face $\mathcal{F} \in \mathcal{F}_h^i$. The face normal points outward of Ω on boundary faces. We consider

a broken polynomial space V_h, which consists of piecewise polynomial functions of d variables (spatial dimension) with the maximum total degree k, $V_h := \mathcal{P}_d^k(\mathcal{T}_h)$, $N_d^k = \dim(\mathcal{P}_d^k(T)) = \frac{(k+d)!}{k!d!}$, $\mathcal{P}_d^k(\mathcal{T}_h) := \{v \in L^2(\Omega) | \, \forall T \in \mathcal{T}_h, v|_T \text{ is polynomial}, \deg(v|_T) \leq k\}$. The usual average and jump operators of a scalar-valued function f_h on interfaces between adjacent elements T_1 and T_2 are defined as $\{\!\{f_h\}\!\} = 0.5(f|_{T_1} + f|_{T_2})$ and $[\![f_h]\!] = f|_{T_1} - f|_{T_2}$. Vector-valued functions are treated component-wise. For boundary faces, we have $\{\!\{f_h\}\!\} = [\![f_h]\!] = f|_T$, when not mentioned otherwise. In the following, first we define the forms a, b, b_{st}, b_{gr} and t, which are used in the weak formulation of the governing equations below. The notation $(\cdot\,,\cdot)$ is used for the $L^2(\Omega)$ inner product of scalar- and vector-valued functions. The Einstein summation convention is considered throughout the paper.

Discrete form of the convective terms

To discretize the convective terms we consider the conservative form with the Lax-Friedrich flux

$$t(\mathbf{u}_h, \mathbf{w}_h, \boldsymbol{\varphi}_h) = -\int_\Omega (\mathbf{u}_h \otimes \mathbf{w}_h) : \nabla \boldsymbol{\varphi}_h + \int_{\mathcal{F}_h} \Big(\{\!\{\mathbf{u}_h \otimes \mathbf{w}_h\}\!\} \cdot \mathbf{n}_\mathcal{F} + \frac{1}{2}\Lambda [\![\mathbf{u}_h]\!] \Big) \cdot [\![\boldsymbol{\varphi}_h]\!],$$

where $\Lambda = \max(\lambda|_{T_1}, \lambda|_{T_2})$ and λ is the absolute eigenvalue of the Jacobian matrix $\Big(\partial[(\mathbf{u} \otimes \mathbf{w}) \cdot \mathbf{n}_\mathcal{F}]/\partial \mathbf{u}\Big)|_{\bar{\mathbf{u}},\bar{\mathbf{w}}}$. The average and jump operators on the Dirichlet boundaries are defined as $\{\!\{\mathbf{u}_h \otimes \mathbf{w}_h\}\!\} = 0.5\Big((\mathbf{u}_h \otimes \mathbf{w}_h)|_T + (\mathbf{u}_D \otimes \mathbf{w}_D)\Big)$, $[\![\mathbf{u}_h]\!] = (\mathbf{u}_h|_T - \mathbf{u}_D)$, $[\![\boldsymbol{\varphi}_h]\!] = \boldsymbol{\varphi}_h|_T$.

Discrete form of the Laplacian of the pressure

To discretize the Laplacian of the pressure we take the following general form using the Symmetric Interior Penalty (SIP) flux

$$a(p_h, q_h) = -\int_\Omega \nabla p_h \cdot \nabla q_h + \int_{\mathcal{F}_h} \Big(\{\!\{\nabla p_h\}\!\} \, [\![q_h]\!] + \{\!\{\nabla q_h\}\!\} \, [\![p_h]\!] \Big) \cdot \mathbf{n}_\mathcal{F} - \int_{\mathcal{F}_h} \mu_p \, [\![p_h]\!] \, [\![q_h]\!] \, .$$

On the Dirichlet boundaries $\mathcal{F} \subset \partial\Omega_D$ we have the boundary condition (5c) $\{\!\{\nabla p_h\}\!\} \cdot \mathbf{n}_\mathcal{F} = \mathbf{n}_\mathcal{F} \cdot \Big(\tilde{\mathbf{u}}_h^{(n)}/\Delta t\Big)$, $[\![p_h]\!] = 0$, $\{\!\{\nabla q_h\}\!\} = \nabla q_h|_T$. In the above discretizations, μ_P is a penalty parameter. The minimal values suggested for the penalty parameter for triangular and tetrahedral meshes can be found in [18, 19] for generic types of elements including hybrid grids. For quadrilateral elements we set

$$\mu_p = \alpha_P c = \begin{cases} \alpha_P \max(c|_{T_1}, c|_{T_2}) & \mathcal{F} \in \mathcal{F}_h^i \\ \alpha_P \, c|_T, & \mathcal{F} \in \mathcal{F}_h^b \end{cases}, \quad c|_T = (k+1)^2 \, \frac{A(\partial T \backslash \mathcal{F}_h^b)/2 + A(\partial T \cap \mathcal{F}_h^b)}{V(T)},$$

where $\alpha_P \geq 1$ is a user defined coefficient to ensure the stability. Area and volume are denoted by A and V, respectively.

Discrete divergence and gradient operators

The divergence of the intermediate velocity $\tilde{\mathbf{u}}_h$ is approximated in the following way

$$b(\tilde{\mathbf{u}}_h/\Delta t, q_h) = -\int_\Omega \tilde{\mathbf{u}}_h/\Delta t \cdot \nabla q_h + \int_{\mathcal{F}_h} \{\tilde{\mathbf{u}}_h/\Delta t\} \cdot \mathbf{n}_\mathcal{F} [\![q_h]\!].$$

We treat the discrete gradient of the pressure component-wise and use the form $b(.,.)$ to define the form $b_{gr}(.,.)$ as follows

$$b_{gr}(p_h, \boldsymbol{\varphi}) = b(p_h \mathbf{e}_i, \varphi_{h,i}) = -\int_\Omega p_h \mathbf{e}_i \cdot \nabla \varphi_{h,i} + \int_{\mathcal{F}_h} \{\!\{p_h\}\!\}\, \mathbf{e}_i \cdot \mathbf{n}_{\mathcal{F}} [\![\varphi_{h,i}]\!].$$

Discrete form for the viscous terms

The discrete form for the viscous term (divergence of the stress tensor), $b_{st}(.,.)$, is defined component-wise using the form $b(.,.)$ by adding a penalty term

$$\begin{aligned} b_{st}(\boldsymbol{\sigma}_h/\rho, \boldsymbol{\varphi}_h) =& b(\sigma_{h,ij}/\rho \mathbf{e}_j, \varphi_{h,i}) - \int_{\mathcal{F}_h} \mu_v \mu_p [\![u_{h,i}]\!]\, [\![\varphi_{h,i}]\!] \\ =& -\int_\Omega \sigma_{h,ij}/\rho \mathbf{e}_j \cdot \nabla \varphi_{h,i} + \int_{\mathcal{F}_h} \{\!\{\sigma_{h,ij}/\rho\}\!\}\, \mathbf{e}_j \cdot \mathbf{n}_{\mathcal{F}} [\![\varphi_{h,i}]\!] - \int_{\mathcal{F}_h} \mu_v \mu_p [\![u_{h,i}]\!]\, [\![\varphi_{h,i}]\!]\,. \end{aligned}$$

On the Dirichlet boundaries $\mathcal{F} \subset \partial\Omega_D$ we have $\{\!\{\sigma_{h,ij}/\rho\}\!\} = (\sigma_{h,ij}/\rho)|_T$, $[\![u_{h,i}]\!] = (u_{h,i}|_T - u_{D,i})$, $[\![\varphi_{h,i}]\!] = \varphi_{h,i}|_T$. Realizing that the stress is a function of the strain, its divergence depends on the second derivatives of the velocity. Therefore, the same penalty term as for the SIP method above is considered here for stability. On the other hand, by adding this penalty term, the no-slip boundary condition is implemented. The penalty parameter μ_p is the same as defined above for the Laplacian of the pressure. The additional penalty parameter μ_v can be set to μ/ρ, where μ is the dynamic viscosity of an equivalent Newtonian fluid.

dG weak formulation of the governing equations

In order to discretize equations (5a)-(5e) in space, we set $\mathbf{u}_h = u_{h,i}\mathbf{e}_i$, $\boldsymbol{\varphi}_h = \varphi_{h,i}\mathbf{e}_i$, where $u_{h,i}$, $\phi_{h,i} \in V_h$, $\mathbf{e}_i$ is the unit vector in direction i, $\boldsymbol{\sigma}_h = \sigma_{h,ij}\mathbf{e}_i\mathbf{e}_j$ and $p_h, q_h \in V_h$,

$$(\widetilde{\mathbf{u}}_h, \boldsymbol{\varphi}_h) = \Delta t\Big(- t(\mathbf{u}_h^{(n)}, \mathbf{u}_h^{(n)}, \boldsymbol{\varphi}_h) + \frac{1}{Re} b_{st}(\boldsymbol{\sigma}_h^{(n)}/\rho, \boldsymbol{\varphi}_h) + (\mathbf{g}_h^{(n)}/\rho, \boldsymbol{\varphi}_h)\Big), \tag{6}$$

$$a(\bar{p}_h^{(n+1)}, q_h) = b(\widetilde{\mathbf{u}}_h/\Delta t, q_h), \tag{7}$$

$$(\widetilde{\widetilde{\mathbf{u}}}_h, \boldsymbol{\varphi}_h) = (\widetilde{\mathbf{u}}_h, \boldsymbol{\varphi}_h) - \Delta t\, b_{gr}(\bar{p}_h^{(n+1)}, \boldsymbol{\varphi}_h), \tag{8}$$

$$(\mathbf{u}_h^{(n+1)}, \boldsymbol{\varphi}_h) = (\mathbf{u}_h^{(n)}, \boldsymbol{\varphi}_h) + (\widetilde{\widetilde{\mathbf{u}}}_h, \boldsymbol{\varphi}_h). \tag{9}$$

4 Hybrid multiscale method (HMM)

To compute the solution of the macroscopic problem, the stress tensor is required at each quadrature point. These data are provided by MD simulations, however, the continuum assumption must still be valid. In dense liquids, MD simulations confirm the continuum assumption up to $2-3\,\mathrm{nm}$ channels [20]. Because of different characteristic values of the microscopic and macroscopic models, adjustments are required for the data transfer between the macroscopic and microscopic simulations. The macroscopic non-dimensional strain $\mathbf{S}$ and stress $\boldsymbol{\sigma}$ tensors are related to the non-dimensional strain $\mathbf{S}_a$

and stress $\boldsymbol{\sigma}_a$ in reduced atomic units in the following way, $\mathbf{S}(u_b/l_b) = \mathbf{S}_a(u_r/l_r)$ and $\boldsymbol{\sigma}(\mu_b u_b/l_b) = \boldsymbol{\sigma}_a(\mu_r u_r/l_r)$. Subscripts b and r correspond to the characteristic values of the box and the reduced atomic units in the particle simulations, respectively. We define $l_a = l_b/l_r$, $u_a = u_b/u_r$, and $\mu_a = \mu_b/\mu_r$ to be the length, velocity, and viscosity of the MD box in the reduced atomic units. For simplicity, we consider $u_a = 1$ and $\mu_a = 1$, and choose $l_a = 10$ for the MD box length. In order to obtain an one-dimensional strain field for the particle simulations we rotate the MD boxes [3]. The following relations apply for the data transfer in 2D hybrid simulations

$$\begin{aligned}\mathbf{S}_a &= \Theta(\mathbf{S}/l_a)\Theta^T \\ &= \frac{1}{l_a}\begin{bmatrix} 0 & \sin(2\theta)(S_{22}-S_{11})/2 + S_{12}\cos(2\theta) \\ \sin(2\theta)(S_{22}-S_{11})/2 + S_{12}\cos(2\theta) & 0 \end{bmatrix},\end{aligned} \tag{10}$$

$$\boldsymbol{\sigma} = \Theta^T(l_a\boldsymbol{\sigma}_a)\Theta, \tag{11}$$

$$\Theta = \begin{bmatrix} \cos(\theta) & \sin(\theta) \\ -\sin(\theta) & \cos(\theta) \end{bmatrix}, \qquad \theta = \frac{1}{2}\tan^{-1}\left(\frac{(S_{22}-S_{11})/2}{S_{12}}\right),$$

4.1 Reduced-order approach

Unknown nonlinear function for stress $\boldsymbol{\sigma}^* = F(\mathbf{S}^*)$ is approximated in the following way

$$\boldsymbol{\sigma}_i^* \approx \widetilde{F}_i(\dot{\gamma}) = \sum_{j=0}^{k} \alpha_{ij}\dot{\gamma}^j, i = \begin{cases} 1,2,3 & \text{2D} \\ 1,..,6 & \text{3D} \end{cases}. \tag{12}$$

Here $\dot{\gamma}$ represents $2S_{12}^*$ for 2D and $2S_{13}^*$ for $3D$ simulations, k is the degree of the approximating polynomial. To reduce a large number of particle simulations we use an offline training phase and an online phase of fast multiple queries. For this training, we solve a least-square problem with the Tikhonov regularization for each component i of the stress tensor

$$\arg\min_x \left(\|Ax-b\|_2^2 + \lambda_1^2\|x\|_2^2 + \lambda_2^2\|Dx\|_2^2\right). \tag{13}$$

Here b is the vector of n ($n \geq k+1$) data points of the corresponding component of the stress tensor obtained by the particle simulations, x is the vector of unknown coefficients. The penalty term Dx is added to damp the oscillations in the derivative function $\partial A/\partial\dot{\gamma}\, x = ADx$. λ_1 and λ_2 are the regularization parameters. The equivalent problem $(A^TA + \lambda_1^2 I + \lambda_2^2 D^TD)x = A^Tb$ is solved by the LU factorization using the LAPACK library [1].

[1] http://www.netlib.org/lapack

Test case 1. We take $\rho = 0.8$ and consider $n = 35$ data points for $\dot{\gamma} \in [0, 1.5]$ to approximate σ_{12}^* for 2D simulations. Least-square problems are solved for λ_1 and λ_2 between 10^{-15} and 10^{-1} and $k = 0, .., 8$. As one can see in Figure 2, we find the optimized solution using the L-curve [21] approach employing a minimum-product corner criterion. The corner of the plot at approximately $(0.005, 3.6)$ represents the optimized solution. The L^2-norm and root-mean-square of the residual of the optimized solution are shown in Table 1 for different degrees k.

Table 1: Numerical convergence of the L^2-norm of the residual for the optimized solution (shown in Figure 2) with respect to the polynomial degree.

k	$\|Ax-b\|_2$	$\|x\|_2$	$\sqrt{(\|Ax-b\|_2^2)/n}$
0	8.029124	0.392878	1.357170
1	0.596365	1.862069	0.100804
2	0.059931	2.655598	0.010130
3	0.033173	2.845212	0.005607
4	0.011536	3.246203	0.001950
5	0.005229	3.838724	0.000884
6	0.005343	3.608710	0.000903
7	0.004903	3.658437	0.000829
8	0.004816	3.467192	0.000814

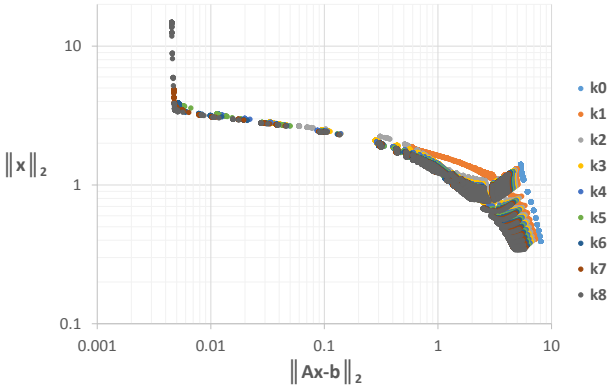

Figure 2: L-curve method to determine the optimized coefficients. L^2-norm of the solution is plotted vs. L^2-norm of the residual for different values of regularization parameters λ_1 and λ_2.

4.1.1 Data refinement strategy

In order to find a proper approximation of the stress tensor with fewer number of particle simulations, we solve the optimization problem above with a relatively small number of samples. Then we use the greedy algorithm (worst scenario search), see e.g. [22], for the data refinement to suggest the shear rate(s) for new particle simulations. If one plots the residual $(Ax - b)$ versus $\dot{\gamma}$, the proposed shear rate for a new simulation $\dot{\gamma}_{new} = 0.5(\dot{\gamma}_M + \dot{\gamma}_N)$, is found in the neighborhood of $\dot{\gamma}_M = \arg\max_{\dot{\gamma}}(Ax - b)$, where $\dot{\gamma}_N$ is the left or right neighbor of $\dot{\gamma}_M$ which corresponds to the larger residual.

4.2 Extension of the approximation

In some cases, the density of the polymers may play a magnificent role. Thus, in order to find the corresponding stress for different densities, we use the extended approximation

$$\boldsymbol{\sigma}_i^* \approx \widetilde{F}_i(\dot{\gamma}, \rho) = \sum_{j_1=0}^{k_1} \sum_{j_2=0}^{k_2} \alpha_{ij_1j_2} \dot{\gamma}^{j_1} \rho^{j_2}, i = \begin{cases} 1,2,3 & \text{2D} \\ 1,..,6 & \text{3D} \end{cases}, \tag{14}$$

where we consider m different density values ρ_l, $l = 1, .., m$ and n_l different shear rates, $l = 1, .., m$. Therefore, the corresponding approximation matrix A has the size $(\sum_{l=1}^{m} n_l) \times \Big((k_1+1)(k_2+1)\Big)$. In order to find the appropriate degrees k_1 and k_2 efficiently, for each density we first find the corresponding approximation as described in Section 4.1. Then, for all densities, k_1 would be the maximum of the degrees of approximation. Now, we start from $k_2 = 0$ and solve for the above approximation in the same way as for approximation (12). We increase k_2 until the residual converges.

4.3 Algorithm for the optimization problem

The following algorithm holds for the case (12) and is applicable to (14), if k_1 is fixed as described in Section 4.2, k_2 is considered as k, and m corresponds to n. Also, extended matrices A, b, and *stderr* (for the standard error of the data) must be used. Depicting $3 \times stderr$, 99% of the samples, which deviate from the (averaged) data points, are taken into account. $k_{\max}$, δ, and ϵ are user-defined parameters.

- Step 1: Set $k = \text{degree}_{\min} = 0$ and $n_{\min} = (\text{degree}_{\min} + 1)$. Consider $n = \max(n_{\min}, N)$, where N is the number of available samples of the parameter, for which the refinement applies. At least $n_{\min}$ samples are required to start the optimization. Set $\text{degree}_{\max} = \min(n, k_{\max})$.

- Step 2: Considering degree k, assemble the corresponding matrix A and solve the least-square problem 13. Set $x_{\text{old}} = x$, $res_{\text{old}} = \text{A}x - b$ and $res_{L^2,\text{old}} = \|x_{\text{old}}\|_2^2$.

- Step 3: Compute $\text{diff} = \|\text{A}x - b\|_2^2 - res_{L^2,\text{old}}$ and $\text{diff}_{\text{rel}} = \text{diff}/\|x_{\text{old}}\|_2^2$. If $\text{diff} < \|stderr\|_2^2$ or $\text{diff}_{\text{rel}} < \delta$ the solution is converged with respect to k. Therefore, set $x = x_{\text{old}}$, $res = res_{\text{old}}$, $res_{L^2} = res_{L^2,\text{old}}$, and $k = k - 1$.

- Step 4: If $res \leq 3 \times stderr$ for each data point, the solution is optimized.

- Step 5: If the solution does not converge or is not optimized, $k = k+1$, assemble A, set $x_{\text{old}} = x$, $res_{\text{old}} = res$, $res_{L^2,\text{old}} = res_{L^2}$ and solve the least-square problem 13.

- Step 6: If $k < \text{degree}_{\max}$ and the solution does not converge and is not optimized, go to Step 3. Otherwise, x is the vector of coefficients and k is the degree of approximation.

- Step 7: Compute $res_{\text{RMS}} = \sqrt{res/n}$. If $res_{\text{RMS}} > \epsilon$ find the new sample for refinement by the worst scenario search (Greedy algorithm), perform the required MD simulations, $N = N + 1$ and go to Step 1. Otherwise, the optimization procedure stops.

Test Case 2. We apply optimization procedure 4.3 to a set of 2D MD data consisting of shear rates $\dot{\gamma} = 0.00, 0.01, ..., 1.00$ to find approximation (12) considering each density

$\rho = 0.1, 0.2, ..., 0.8$. Parameters λ_1 and λ_2 are between 10^{-15} and 10^{-2}, and $\delta = 0.05$. The refinement Step 7 of the algorithm is excluded. The coefficients are shown in Table 2 for $\rho = 0.5$ as an example. The coefficient α_1 can be considered as the viscosity of an equivalent Newtonian fluid. The coefficients α_0 of the normal components of the stress are used to compute the pressure as one half of the trace of the stress tensor. The fluid pressures calculated in this way for different densities are compared with the Henderson equation of state for hard disks in Figure 3.

Table 2: Coefficients of approximation (12) using 2D MD data at density $\rho = 0.5$.

	σ_{11}	σ_{12}	σ_{22}
α_0	-1.559856	0.019031	-1.524225
α_1		0.516020	
$\text{Residual}_{\text{rms}}$	0.044120	0.008918	0.016566

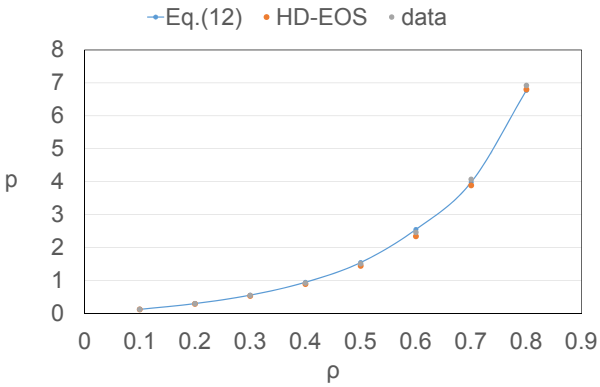

Figure 3: Pressure from the mean stress in 2D MD in comparison with the Henderson equation of state for hard-disks and approximation (12).

Test Case 3. We apply optimization procedure 4.3 to a set of 3D MD data to find approximations (12) and (14). The data set consists of 48 data points of 12 shear rates $\dot{\gamma} = 0.0, 0.001, 0.005, 0.01, 0.025, 0.033, 0.05, 0.066, 0.075, 0.1, 0.5, 1.0$ and densities $\rho = 0.4, 0.5, 0.6, 0.8$. The same numerical settings as in Test case 2 are used, parameters λ_1 and λ_2 are between 10^{-15} and 10^{-2} and $\delta = 0.05$. The refinement Step 7 of the algorithm is excluded. The coefficients of approximation (12) are shown in Tables 3 for $\rho = 0.5$. The coefficients of approximation (14) are shown in Table 4. The pressures as one third of the trace of the stress tensor found from approximations (12) and (14) are compared with the Carnahan-Starling equation of state for hard spheres in Figure 4.

Table 3: Coefficients of approximation (12) using 3D MD data for $\rho = 0.5$.

	σ_{11}	σ_{12}	σ_{13}	σ_{22}	σ_{23}	σ_{33}
α_0	-1.702695	-0.000039	0.002679	-1.698915	-0.000216	-1.739654
α_1			0.438956			
$\text{Residual}_{\text{rms}}$	0.038215	0.000160	0.002336	0.030139	0.000498	0.030025

Table 4: Coefficients of approximation (14) using 3D MD data.

	σ_{11}	σ_{12}	σ_{13}	σ_{22}	σ_{23}	σ_{33}
α_{00}	-3.543503	-0.0000013	0.007578	-3.767376	-0.000019	-3.746758
α_{10}			0.519910			
α_{01}	16.503534		0.042466	17.262241		16.961379
α_{11}			-1.421053			
α_{02}	-25.455935		-0.196039	-26.026600		-25.708823
α_{12}			1.0097451			
α_{03}			0.179535			
α_{13}			2.939758			
$\text{Residual}_{\text{rms}}$	0.090635	0.000001	0.006968	0.060957	0.000394	0.084390

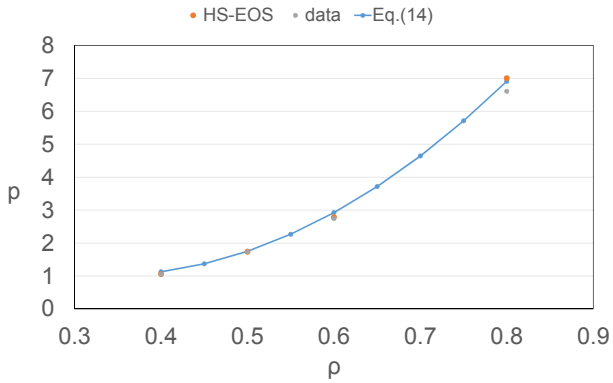

Figure 4: Pressure from the mean stress in 3D MD in comparison with the Carnahan-Starling equation of state for hard-spheres and approximation (14).

5 Reduced-order hybrid simulations

Two-dimensional hybrid simulations of the Couette flow are performed using the 2D MD data for $\rho = 0.5$ from Test case 2. Here we apply the optimization algorithm including the refinement Step 7 according to Section 4.1.1 to find approximation (12) with the greedy refinement strategy. The levels of refinement are shown in Figure 5. We start with 4 data points, which are shown in Table 5. The refinement procedure terminates after 10 levels including 23 data points out of 101 total data points. The best approximation for σ_{12} is found after 3 levels of refinement including 10 data points. However, if one considers all components of the stress, the best approximation would be the one from the first level with 6 data points. Note that one should stop the refinement algorithm at this level in order to avoid considering data points with higher statistical errors. The coefficients using 6 and 10 data points are shown in Table 5, which are similar to the coefficients in Table 2 using all data points. Therefore, we choose $\alpha_1 = 0.516$ as the viscosity of the equivalent

Table 5: Coefficients of approximation (12) for 2D MD data at $\rho = 0.5$ applying the refinement shown in Figure 5.

Starting values, $\dot{\gamma} = \{0.0, 0.25, 0.75, 1.0\}$

	α_0	α_1	$\text{Residual}_{\text{rms}}$
σ_{11}	-1.566603		0.057684
σ_{12}	0.011217	0.515426	0.010882
σ_{22}	-1.528000		0.022316

6 values, $\dot{\gamma} = \{0.0, 0.25, 0.75, 0.87, 0.88, 1.0\}$

	α_0	α_1	$\text{Residual}_{\text{rms}}$
σ_{11}	-1.582399		0.053632
σ_{12}	0.011120	0.516600	0.008897
σ_{22}	-1.534684		0.020448

10 values, $\dot{\gamma} = \{0.0, 0.06, 0.12, 0.13, 0.5, 0.6, 0.65, 0.75, 0.94, 1.0\}$

	α_0	α_1	$\text{Residual}_{\text{rms}}$
σ_{11}	-1.564935		0.058747
σ_{12}	0.010471	0.516323	0.007196
σ_{22}	-1.528257		0.022103

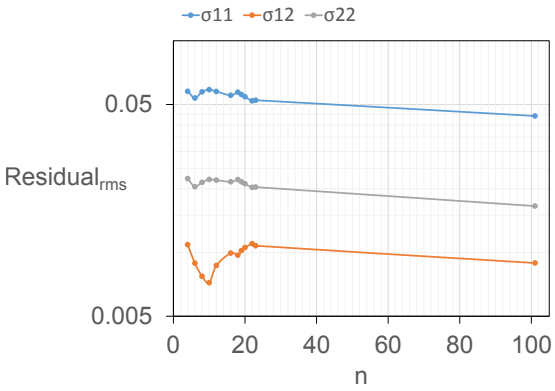

Figure 5: Optimization algorithm including the greedy data refinement strategy.

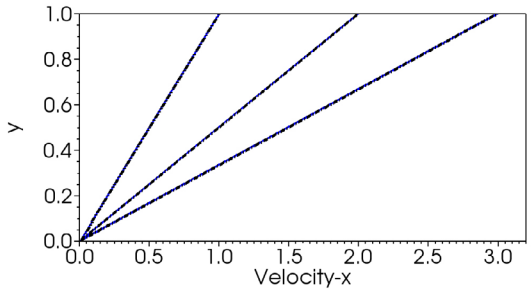

Figure 6: Velocity profiles in the streamwise direction for shear velocities $U = 1, 2, 3$. Blue solid lines: hybrid simulations, black dash-dot lines: analytic solutions $u_x = yU$.

Newtonian fluid with the same density $\rho = 0.5$ for comparison.

The macroscopic hybrid simulations of the Couette flow are performed on the domain $[-1, 1] \times [0, 1]$. The flow is periodic in the streamwise x-direction. The no-slip boundary condition is applied at the walls. At the lower wall $y = 0$, the velocity is zero. At the upper wall $y = 1$, the velocity in x-direction is equal to U and the velocity in y-direction is zero. A grid of 3×3 cells is employed. A polynomial degree $k = 1$ is assigned in the dG method, $Re = 1$. The velocity profiles presented in Figure 6 overlap with the analytical solution $u_x = yU$ for the equivalent Newtonian fluid with density $\rho = 0.5$ and viscosity $\mu = 0.516$.

Three-dimensional hybrid simulations of the Poiseuille flow are performed using approximation (14) to the 3D MD data in Test case 3. The approximation coefficients are shown in Table 4. We take the corresponding coefficients of σ_{13} to estimate the viscosity of the equivalent Newtonian fluid using relation $\mu = \alpha_{10} + \alpha_{11}\rho + \alpha_{12}\rho^2 + \alpha_{13}\rho^3$. The viscosities for different densities are listed in Table 6 and plotted in Figure 7. The viscosi-

Table 6: Estimates of the Newtonian fluid viscosity $\mu = \lim_{\dot{\gamma}\to 0} |\sigma_{13}/\dot{\gamma}|$ using approximations (12) and (14) with 3D MD data.

	Eq.(12)	Eq.(14)
0.4	0.301957	0.301193
0.45	0.352795	
0.5	0.438956	0.429290
0.55		0.532881
0.6	0.649864	0.665775
0.65		0.830174
0.7		1.028285
0.75		1.262313
0.8	1.537902	1.534461

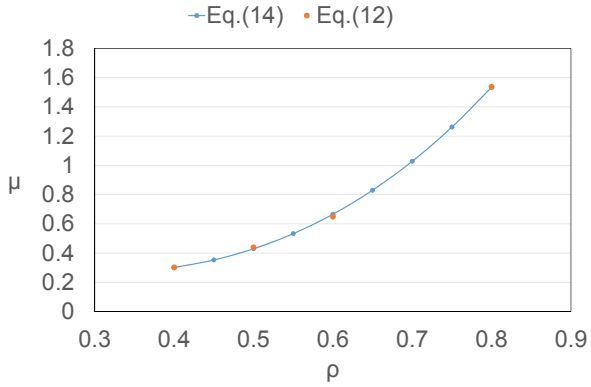

Figure 7: Estimated Newtonian fluid viscosity vs. density in 3D MD.

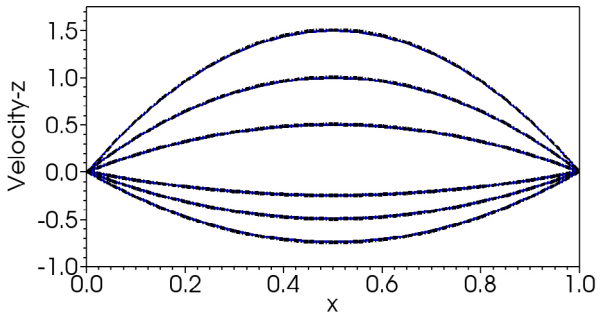

Figure 8: Velocity profiles in the streamwise direction for pressure gradient parameter $P = -3, -2, -1, 2, 4, 6$. Blue solid lines: hybrid simulations, black dash-dot lines: analytic solutions $u_z = x(1-x)P$.

ties obtained from approximations (12) and (14) match very well. The hybrid simulations are performed for $\rho = 0.55$, for which we do not have the MD data. The computational domain is taken as $[0,1]\times[-1,1]\times[-1,1]$. The flow is periodic in y- and z-directions. The no-slip boundary condition is applied at the walls $x = 0$ and $x = 1$, where the velocity is zero. The pressure gradient $f_z = -2\mu\, P/Re$ is applied in the streamwise z-direction with $Re = 1$. We estimate the viscosity of the equivalent Newtonian fluid $\mu = 0.53$. A grid of $3\times 3\times 3$ cells is employed. The polynomial degree is $k = 2$ in the dG method. Velocity profiles in z-direction are plotted for different values of the pressure gradient parameter P in Figure 8.

6 Acknowledgments

The present work is supported by German Science Foundation (DFG) under the grant TRR 146. We would like to thank M. Oberlack, F. Kummer and B. Müller for providing their code BoSSS. The authors gratefully acknowledge the computing time granted on the HPC cluster Mogon at Johannes Gutenberg-University Mainz.

REFERENCES

[1] W. E and B. Enquist. The heterogeneous multiscale methods. *Commun. Math. Sci.*, 1(1):87–132, 2003.

[2] W. Ren and W. E. Heterogenous multiscale method for the modeling of complex fluids and micro-fluidics. *J. Comput. Phys.*, 204:1–26, 2005.

[3] Sh. Yasuda and R. Yamamoto. A model for hybrid simulations of molecular dynamics and computational fluid dynamics. *Phys. Fluids*, 20(11):113101, 2008.

[4] W. E, W. Ren, and E. Vanden-Eijnden. A general strategy for designing seamless multiscale methods. *J. Comput. Phys.*, 228(15):5437–5453, 2009.

[5] M.K. Borg, Lockerby D.A., and J.M. Reese. A hybrid molecular–continuum method for unsteady compressible multiscale flows. *J. Fluid Mech.*, 768:388–414, 2015.

[6] D. Frenkel and B. Smit. *Understanding Molecular Simulations.* Academic Press, 1996.

[7] A. W. Lees and S. F. Edwards. The computer study of transport processes under extreme conditions. *J. Phys. C.*, 5:1921–1929, 1972.

[8] C. P. Lowe. An alternative approach to dissipative particle dynamics. *Europhys. Lett.*, 47:145–151, 1999.

[9] P. J. Daivis and B. D. Todd. A simple, direct derivation and proof of the validity of the SLLOD equations of motion for generalized homogeneous flows. *J. Chem. Phys.*, 124:194103, 2006.

[10] J. H. Irving and J. G. Kirkwood. The statistical mechanical theory of transport processes. iv. the equations of hydrodynamics. *J. Chem. Phys.*, 18:817, 1950.

[11] B. Sanderse and B. Koren. Accuracy analysis of explicit Runge-Kutta methods applied to the incompressible Navier-Stokes equations. *J. Comput. Phys.*, 231(8):3041–3063, 2012.

[12] G. A. Reis, I. V. M. Tasso, L. F. Souza, and J. A. Cuminato. A compact finite differences exact projection method for the Navier-Stokes equations on a staggered grid with fourth-order spatial precision. *Comput. Fluids*, 118:19–31, 2015.

[13] S. A. Orszag, M. Israeli, and M. O. Deville. Boundary conditions for incompressible flows. *J. Sci. Comput.*, 1:75–111, 1986.

[14] E. Ferrer, D. Moxey, R. H. J. Willden, and S. J. Sherwin. Stability of projection methods for incompressible flows using high order pressure-velocity pairs of same degree: continuous and discontinuous Galerkin formulations. *Commun. Comput. Phys.*, 16(3):817–840, 2014.

[15] D. T. Steinmoeller, M. Stastna, and K. G. Lamb. A short note on the discontinuous Galerkin discretization of the pressure projection operator in incompressible flow. *J. Comput. Phys.*, 251:480–486, 2013.

[16] N. Emamy. *Numerical simulation of deformation of a droplet in a stationary electric field using DG*. PhD thesis, TU Darmstadt, Darmstadt, 2014.

[17] D. A. Di Pietro and A. Ern. *Mathematical Aspects of Discontinuous Galerkin Methods*. Springer-Verlag Berlin Heidelberg, 2012.

[18] K. Shahbazi. An explicit expression for the penalty parameter of the interior penalty method. *J. Comput. Phys.*, 205(2):401–407, 2005.

[19] K. Hillewaert. *Development of the discontinuous Galerkin method for high-resolution, large scale CFD and acoustics in industrial geometries*. Ph.D. thesis, Université catholique de Louvain, 2013.

[20] D. M. Holland, M. K. Borg, D. A. Lockerby, and J. M. Reese. Enhancing nano-scale computational fluid dynamics with molecular pre-simulations: Unsteady problems and design optimisation. *Comput. Fluids*, 115:46–53, 2015.

[21] P. Ch. Hansen and D. P. O'Leary. The use of the L-curve in the regularization of discrete ill-posed problems. *SIAM J. Sci. Comput.*, 14(6):1487–1503, 1993.

[22] V. N. Temlyakov. Greedy approximation. *Acta Numer.*, 17:235–409, 2008.